

A Network Science Approach to Granular Time Series Segmentation

Ivana Kesić¹, Carolina Fortuna¹, Mihael Mohorčič¹, and Blaž Bertalanič^{1*}

¹Jožef Stefan Institute, SI-1000 Ljubljana

*blaz.bertalanic[at]ijs.si

ABSTRACT

Time series segmentation (TSS) is one of the time series (TS) analysis techniques, that has received considerably less attention compared to other TS related tasks. In recent years, deep learning architectures have been introduced for TSS, however their reliance on sliding windows limits segmentation granularity due to fixed window sizes and strides. To overcome these challenges, we propose a new more granular TSS approach that utilizes the Weighted Dual Perspective Visibility Graph (WDPVG) TS into a graph and combines it with a Graph Attention Network (GAT). By transforming TS into graphs, we are able to capture different structural aspects of the data that would otherwise remain hidden. By utilizing the representation learning capabilities of Graph Neural Networks, our method is able to effectively identify meaningful segments within the TS. To better understand the potential of our approach, we also experimented with different TS-to-graph transformations and compared their performance. Our contributions include: a) formulating the TSS as a node classification problem on graphs; b) conducting an extensive analysis of various TS-to-graph transformations applied to TSS using benchmark datasets from the TSSB repository; c) providing the first detailed study on utilizing GNNs for analyzing graph representations of TS in the context of TSS; d) demonstrating the effectiveness of our method, which achieves an average F1 score of 0.97 across 59 diverse TSS benchmark datasets; e) outperforming the seq2point baseline method by 0.05 in terms of F1 score; and f) reducing the required training data compared to the baseline methods.

1 Introduction

In today's digital era, time series (TS) are one of the most frequently encountered data types. Low-cost, high-resolution sensors have become a key part in mobile devices, industrial monitoring and healthcare, producing large amounts of TS data that capture the temporal patterns and essential statistical properties of various processes or phenomena¹. With the rapid progress in automatic data acquisition and storage, we are now faced with the challenge of data that far exceeds our comprehension. TS analysis methods such as clustering, classification or regression, are therefore essential for effective and efficient processing of TS data^{2–5}. Although these methods are crucial, they often benefit from first segmenting the TS into smaller, more manageable parts, through a process known as Time Series Segmentation (TSS). It first involves *identifying critical time points* dividing the TS into smaller segments and second *label them based on activity*. This segmentation step can significantly simplify subsequent tasks such as classification or anomaly detection and provide more targeted insights. For example, in the field of telecommunications⁶ the increasing volume of the network traffic data is a constant challenge. With TSS, we can segment network traffic, making it easier to detect patterns and respond swiftly to potential issues, such as peak usage periods, while optimizing bandwidth efficiency.

In recent years, deep learning (DL)^{7,8} architectures have been introduced as a TSS method, however they have not yet reached the same level of performance in TSS as in other fields such as computer vision. Many of these approaches rely on sliding-window techniques, where the TS is partitioned into evenly sized segments that are individually labeled before being recombined. While sliding-window methods yield satisfactory results, they limit the granularity of segmentation due to fixed window sizes and strides.

A different, less mainstream approach to TS analysis, explores graphs as a viable TS representation^{9–12} where each value in the raw TS is represented as a node. Transforming TS into graphs not only preserves the temporal order of the data, but also reveal interactions and dependencies between non consecutive points, which is important for tasks such as TSS. This transformations enables the adoption of Graph Neural Networks (GNNs), which are particularly well-suited to learn complex structural features. GNNs can help identify the critical transition points that distinguish different segments, and are able to capture subtle temporal dependencies and variations that often precede significant changes in the TS. Such representations based on node density and message passing between node neighborhoods naturally eliminate the fixed window sizes and strides from DL.

By considering the combination of TS graph representations and GNNs, and taking inspiration from the dense labeling approach in computer vision where every pixel is assigned a class label¹³, we can reformulate the TSS challenge as a node-level classification problem. In our graph representation of TS data, dense labeling entails assigning a specific label to each node, ensuring that even the most subtle transitions are detected and appropriately classified. In this work we aim to conduct a comprehensive and robust exploration of the different graph representations for TSS on the TSSB benchmark datasets in combination with GNNs. Based on the findings of this exploration, we propose a new approach that combines the Weighted Dual Perspective Visibility Graph (WDPVG) transformation with a GAT-based GNN architecture. The contributions of this paper are as follows:

- We formulate the TSS as a node classification problem on graphs
- We perform an extensive study on the suitability of several TS to graph transformations for TSS on TSSB benchmark datasets
- We perform a first-time analysis of TS graph representation for TSS with GNNs
- We show that our proposed approach achieves an average F1 score of 0.97 on 59 different open source TSS benchmark datasets from different domains
- We show that our proposed method outperforms the baseline seq2point method by 0.05 in F1 score
- We show that the proposed method requires significantly less training data for training compared to the baseline.

This paper is organized as follows. The related work is discussed in Section 2. Section 3 provides the problem formulation, while Section 4 elaborates on the proposed time series transformation. Section 5 introduces the proposed deep learning architecture, Section 6 describes the relevant methodological and experimental details, while Section 7 provides thorough analysis of the results. Finally, Section 8 concludes the paper.

2 Related work

Time series segmentation (TSS) is the task of partitioning time series into distinct, non-overlapping segments, each corresponding to an underlying state or pattern. Research in this area can be broadly categorized into three main categories depending on its application, as illustrated in Figure 1: Change Point Detection (CPD), which seeks to identify the specific time points of change; Windowed Segment Classification (WSC), which classifies fixed-length windows of the series; and Dense Labeling or Precise Segmentation (DLPS), which assigns a class label to every individual time step.

As summarized in Table 1, these approaches have increased in complexity to address the limitations of earlier methods. The table lists key research works in the first column, followed by columns detailing the problem type addressed, the data type used, the number of datasets, and the core methodology employed.

Work	Problem Type	Data Type	No. of Datasets	Methodology
Arif et al. ¹⁴	CPD	UTS	1	Statistical (CUSUM)
Ermshaus et al. ¹⁵	CPD	UTS	75	ML (k-NN Classifier)
De Ryck et al. ¹⁶	CPD	UTS	5	DL (Autoencoder)
Perslev et al. ⁷	WSC	MTS	7	DL (U-Time CNN)
Gaugel et al. ¹⁷	DLPS	MTS	1	DL (CNN-LSTM)
This Work	DLPS	UTS (Graph)	59	DL (GNN)

Table 1. Summary of key related works.

Early research predominantly focused on CPD. Initial approaches relied on statistical methods, such as those used by Arif et al.¹⁴ to analyze climate data. Their methodology employed two statistical techniques: Cumulative SUM (CUSUM) to detect shifts in climate patterns, and bootstrapping to confirm the significance of those shifts. However, these statistical methods often struggle with subtle changes in autocorrelation or suffer from high false-alarm rates. This motivated the development of machine learning and deep learning solutions. For instance, De Ryck et al.¹⁶ employed a deep autoencoder to learn a stable, time-invariant representation of the time series. Change points are then identified by calculating a dissimilarity measure (e.g., the Euclidean distance) between consecutive windows' feature representations, where notable increases in this measure indicate potential change points. In a different deep learning approach, Ermshaus et al.¹⁵ framed CPD as a self-supervised classification

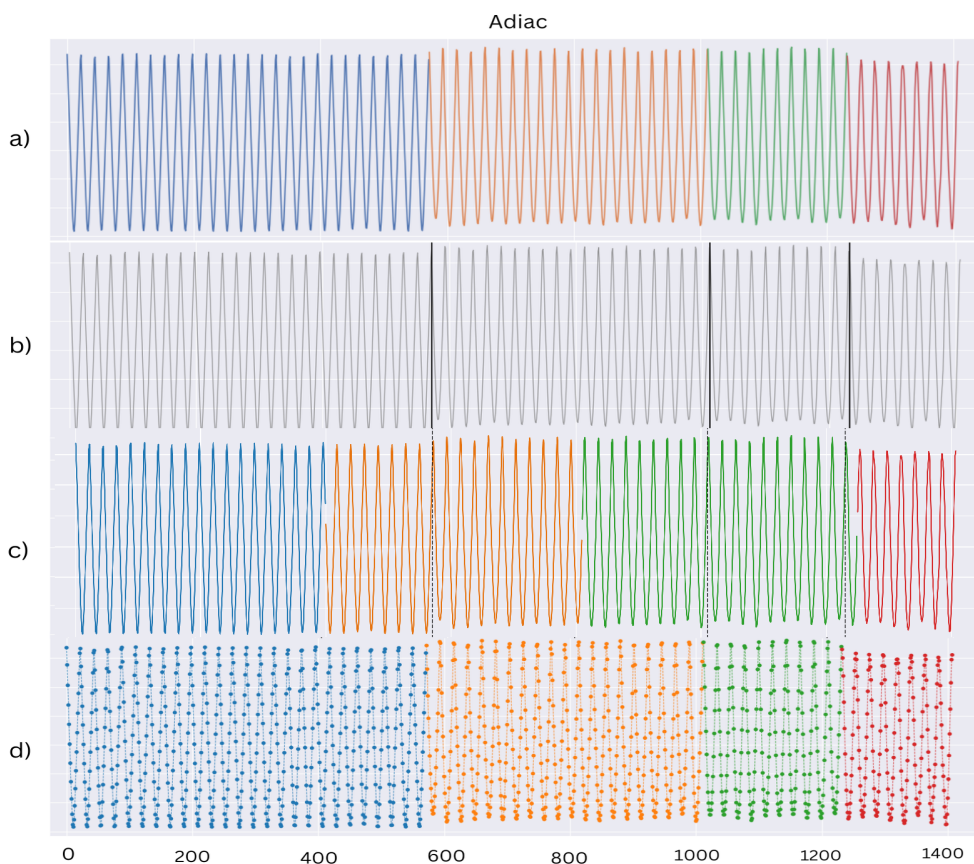


Figure 1. Example of three existing segmentation categories for the Adiac TSSB dataset. a) Ground truth, b) CPD, c) WSC, d) DLPS

problem. Their method, ClaSP, uses a binary k-NN classifier to partition a time series recursively. For each potential split point, the classifier is trained to distinguish between the two resulting segments, and the split point yielding the highest accuracy is selected. ClaSP further automates this process by determining its own hyperparameters from the data, removing the need for manual tuning.

However, a key limitation of CPD lies in its inability to classify the underlying nature of each segment. Consequently, TSS has evolved into a classification problem to overcome this gap. The most common strategy is WSC, in which the time series is split into fixed-length windows, each labeled independently. For instance, Perslev et al.⁷ employed a CNN-based U-Time architecture to segment sleep stages in EEG signals. A drawback, however, is that segmentation granularity depends on the chosen window size. Reducing the window to a single time stamp yields the most granular approach, referred to as DLPS. Gaugel et al.¹⁷ introduced a deep learning model that merges sliding window and dense labeling techniques by employing CNNs for intra-window feature extraction, LSTM networks for inter-window contextual understanding, and a refinement module for dense labeling. Evaluated on multivariate time series with their model achieved a segmentation accuracy of approximately 96%.

This evolution reveals a clear and critical research gap, as shown in Table 1. While CPD for univariate time series (UTS) is well-explored, the more advanced WSC and DLPS methods have been overwhelmingly applied to multivariate time series (MTS)^{7,17}. The rich, multi-channel information in MTS data provides a strong feature basis for complex DL models. Univariate data lacks this explicit dimensionality, making it far more challenging to capture the complex temporal dependencies required for dense labeling.

To address this gap, our work formulates a novel approach to the DLPS of univariate data. We propose a dimensionality expansion technique that transforms the 1D time series into a graph representation. This allows us to leverage the powerful relational learning capabilities of Graph Neural Networks (GNNs). To the best of our knowledge, this work is the first to apply a GNN-based framework to the precise, dense labeling segmentation of univariate time series.

3 Problem formulation

TSS as a fundamental task in time series analysis involves partitioning a sequence into semantically meaningful segments. In this work, we formulate TSS as a point-wise classification problem, also referred to as DLPS, where each time step in a time series is assigned a categorical label indicating its segment membership. This formulation aligns well with graph node classification tasks¹⁸. By representing the TS as a graph, where each time point corresponds to a graph node, the task of segmenting the series translates to assigning labels to these nodes.

Let S be a univariate time series of length N :

$$S = \{s_1, s_2, \dots, s_N\}, \quad s_i \in \mathbb{R} \quad (1)$$

where each s_i represents a value of the TS at time step i . The objective of TSS is to assign a label y_i to each time point s_i , where the label corresponds to one of C predefined segment classes:

$$Y = \{y_1, y_2, \dots, y_N\}, \quad y_i \in \{0, 1, \dots, C\} \quad (2)$$

To assign the labels, we first construct a corresponding TS graph representation through a transformation function $T(S)$, i.e., $G = T(S)$. The resulting graph $G = (V, E)$ encapsulates the link dynamics of TS S , where:

- $V = \{v_1, v_2, \dots, v_N\}$ is the set of nodes, where each node v_i represents a time step s_i .
- $E \subseteq V \times V$ is the set of edges that define the structural relationships between time points.

Given the graph G , the goal of TSS is to assign a segment label y_i to each node (i.e., time step). The segmentation task is then defined as node classification function F_G over the graph:

$$y_i = F_G(G; \theta)_i \quad (3)$$

where θ represents the model parameters. This formulation aims to provide continuous and dense labeling across all time steps, enabling fine-grained segmentation.

4 Time series to graph transformations

In this section, we describe the main data preparation step, how to transform TS into graphs. We define the transformation $T()$ that transforms the input TS S to its corresponding graph G : $G = T(S)$. Each node in the graph corresponds to a time stamp in the TS, while the edges between them represent their relationships. To determine the set of edges, Silva et al.¹⁹ collected and presented three classes of approaches according to the underlying mapping concepts: the Visibility Graph Transformations, the Transition Networks and the Proximity Networks. Table 2 provides a comparative overview of these transformation methods. The first column lists all the variants that were utilised in this work. The second column specifies the node representation used in each algorithm, where t denotes time points, while q_i , π_i or \vec{z}_i correspond to state based representations of the time points. The third column describes the edge type, such as Natural Visibility (NV) and Horizontal Visibility (HV) edges in Visibility Networks, Transition Probability (TP) edges indicating probability based connections, and Distance based Measure (DM) edges in Proximity Networks. The fourth and fifth columns indicate whether the generated networks have directed and weighted edges.

	Network type	node	edge	directed	weighted
VISIBILITY	Natural Visibility Graph (NVG)	t	NV	✗	✗
	Horizontal Visibility Graph (HVG)	t	HV	✗	✗
	Directed NVG	t	NV	✓	✗
	Directed HVG	t	HV	✓	✗
	Weighted NVG	t	NV	✓	✓
	Weighted HVG	t	HV	✓	✓
	Weighted Dual Perspective Visibility Graph	t	NV	✓	✓
TRANSITION	Quantile Network	q_i	TP	✓	✓
	Ordinal Partition Transition Network	π_i	TP	✓	✓
	Coarse-Grained Phase Space Graph	\vec{z}_i	TP	✓	✓
PROXIMITY	k-NN Network	\vec{z}_i	DM	✓	✓

Table 2. Comparison of Network Types

4.1 Visibility Networks

The visibility transformations from TS to complex networks are based on traditional visibility algorithms from computational geometry²⁰, associated with the natural ordering of the TS. In Table 2 we listed the algorithms that were utilised in this work.

The Natural Visibility Graph (NVG), originally introduced by Lacasa et al.¹⁰, is based on the concept of visibility. In the NVG, each data point in the TS is treated as a vertical bar whose height corresponds to its value. Two points are connected if the line of sight between them is not obstructed by any intermediate data point. This means that there is a direct line of sight between the bars without any interception. Expressed mathematically: If any two points (t_i, s_i) and (t_j, s_j) have visibility, the following condition applies to every point (t_k, s_k) in between:

$$s_k < s_i + \frac{(s_j - s_i)(t_k - t_i)}{(t_j - t_i)}, \quad i < k < j$$

where: t_i , t_j and t_k are the time coordinates of the points, while s_i , s_j and s_k are the TS values at these specific time coordinates. The created edges e are stored in an adjacency matrix A^{NVG} . The NVG algorithm is easy to implement and has quadratic complexity $O(S^2)$ ¹⁹ in terms of computational complexity. However, the NVG algorithm has two disadvantages, as it does not take into account the effect of uneven TS sampling and does not capture TS changes when the values are negative.

To overcome these disadvantages, a variation of NVG called the Weighted Dual Perspective Visibility Graph (WDPVG) was proposed by Zheng et al.⁹. According to the authors, the WDPVG method deals with uneven sampling in the time series by

explicitly assigning weights to edges between nodes based on metrics such as Euclidean distance, tangent of the viewing angle, or actual time differences between connected points. Additionally, WDPVG captures both peaks and troughs of the time series, by incorporating a dual perspective, which is achieved by combining the NVG with its reflected counterpart. To compute the reflected perspective of the NVG (RPNVG), the time series is inverted by mirroring its values on the time axis, resulting in a new series $S'_{1 \times N} = -S_{1 \times N}$. A NVG is then constructed on this inverted series, resulting in an additional adjacency matrix A_{RPNVG} , which adds new edges $e_{i,j}$.

The final adjacency matrix for WDPVG, A_{WDPVG} , is created by combining the original NVG matrix and the RPNVG matrix using the rule:

$$A_{WDPVG_{i,j}} = \max(A_{NVG_{i,j}}, A_{RPNVG_{i,j}})$$

The resulting graph $G = (V, E)$ is defined by the nodes $v_n \in V$, representing each measurement s_N in the time series, and the edges $e_{i,j} \in E$, stored in the adjacency matrix A_{WDPVG} .

Another version of the VG proposed by Luque et al.¹¹ is called the Horizontal Visibility Graph (HVG). Here, the visibility between two points is determined by a horizontal criterion. In a HVG, two nodes v_i and v_j are connected if all intermediate nodes v_k satisfy the following condition:

$$s_i, s_j > s_k, \quad \forall k \in (i, j)$$

The HVG is simpler and computationally more efficient than the NVG. Because of the limiting visibility criteria it does not capture as much information as the NVG does, but it is suitable when a quick, lightweight graph representation is needed.

The Weighted¹² and Directed²¹ Visibility Graphs are modifications of the core NVG or HVG, created by adding specific parameters to extend their functionality. By adding one of the two direction values: left to right (edge direction go from left to right according to the series temporal axis, which preserves the natural, temporal order of TSs) or top to bottom (edge directions go from top to bottom according to the value axis, focusing on magnitude differences between data points), we obtain a directed graph. Additionally, each edge in the graph going from one point to another can be associated with a feature vector or weight, denoted as w_{ij} . The 'weighted' parameter can take one of the following values: Euclidean distance, squared Euclidean distance, horizontal or vertical distance and their absolute variants, slope, and absolute slope. The edges together with their weight values are stored in the adjacency matrix A.

4.2 Transition Networks

Transition Networks can be seen in rows 9 to 11 in Table 2. They are created by converting sequences of data points from the TS into symbols (states), and mapping the symbols and transitions between them into nodes and edges, respectively. The construction of this type of network involves two steps. First, the TS is partitioned into k symbols (or states) $q = \{q_1, q_2, \dots, q_k\}$ based on a chosen strategy, such as quantile partitioning or phase space reconstruction. Each data point s_i in the TS $S = \{s_1, s_2, \dots, s_N\}$ is mapped to a symbol q_j using a partitioning function:

$$q_j = f(s_i), \quad f: \mathbb{R} \rightarrow Q$$

Here, $f(s_i)$ assigns a symbol to each data point based on its value. As summarized in Table 2, these networks are typically directed and weighted, with the edges capturing the frequency of transitions between the states, and by that the resulting network represents the dynamics of the TS. The corresponding adjacency matrix is a Markov transition field (MTF) matrix A_{MTF} , given by :

$$A_{MTF,i,j} = \begin{cases} A_{s_i,s_j} & \text{if } i \leq j, \\ 0 & \text{otherwise} \end{cases}$$

where A_{s_i,s_j} represent the probability of transitioning from state q_j to state q_i , and i and j are indices of the time series data points, mapped to their corresponding states q .

The computational complexity of the MTF increases quadratically with the length of the TS. Since the average length of the TS data in our benchmark datasets exceeds 3000, the application of the MTF becomes prohibitively expensive. Three main examples of this network type are Quantile Graphs²², Ordinal Partition Transition Networks (OPTN) and Coarse-Grained Phase Space Graphs(CGPS).

4.3 Proximity Networks

The utilised type of the Proximity Network can be seen in the last row in Table 2. The proximity concept, on which these networks are based on, means that the measure of distance $d(s_i, s_j)$ or similarity (correlation) $r(s_i, s_j)$ is used to calculate the distance between the points in the TS incorporated in the multidimensional phase space. Nodes in this network represent the states of the TS, and edges are established based on the chosen distance or similarity metric. For example, the utilised k-NN network as shown in Table 2, has edges based on the measure of distance between the nodes. The ability to connect different nodes based on proximity measures allows capturing meaningful information about the topology of dynamical systems, enabling to identify different regimes or patterns along the series²³. The adjacency matrix for this type of network can, in general, be written as:

$$A_{i,j} = \begin{cases} 1 & \text{if } d(s_i, s_j) \leq \epsilon \text{ or } r(s_i, s_j) \geq \alpha \text{ (binary matrix),} \\ w_{i,j} & \text{if proximity measure is used and weighting is applied,} \\ 0 & \text{otherwise.} \end{cases}$$

Proximity networks include cycle networks²⁴²⁵, correlation²⁶ and recurrence networks²⁷.

5 Proposed segmentation model

In this section, we describe our proposed model. As described in Section 3, our goal is a point-wise classification task, where a class must be assigned to each point in the TS. After transforming the TS into a graph representation, as described in Section 4, our point-wise classification task converts into a node classification task. In other words, each node in the graph corresponds to a time point, and we predict a label for each node. Formally, we define our prediction model as a function Φ , which transforms the input data G to the set of target classes $Y_{1 \times N}$:

$$\Phi : G \rightarrow Y_{1 \times N}$$

5.1 Proposed GNN model

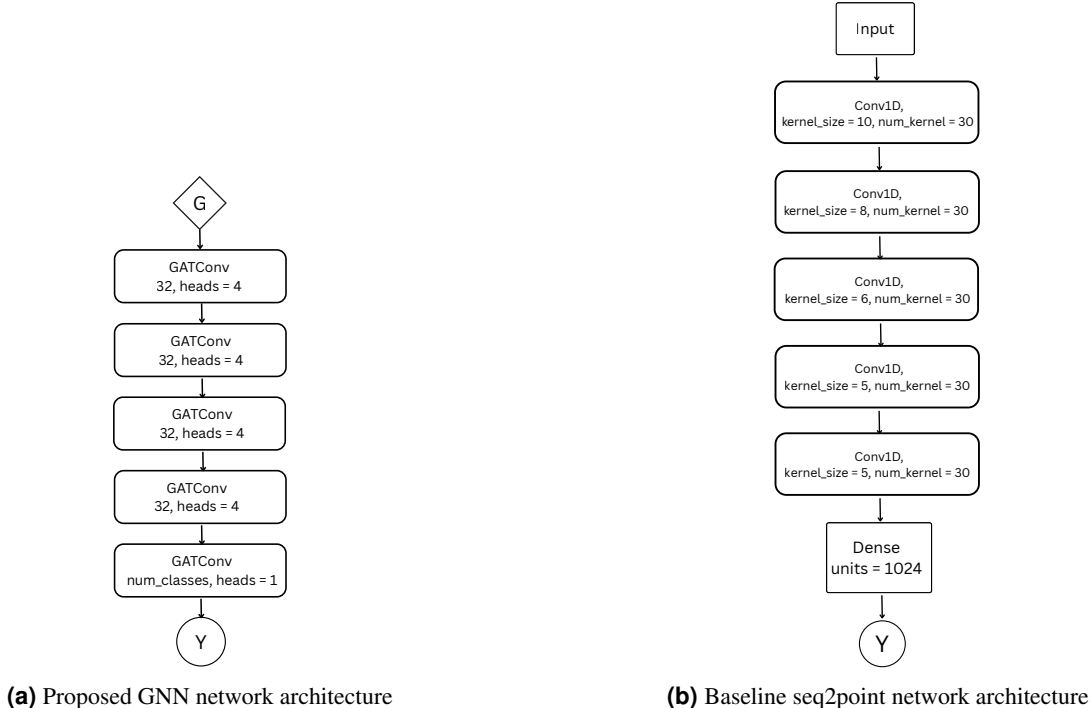


Figure 2. Comparison of network architectures for TS segmentation

To realize the function $F_G()$, from Eq. 3 to predict target classes from the transformed graph data denoted as G , a Graph Neural Network was designed based on the Graph Attention Networks (GAT)²⁸. The main advantage of GAT is its self-attention

mechanism on node features, which significantly improves classification performance in node classification tasks. This mechanism enables the model to compute attention scores between nodes and their neighbors, determining the influence each neighboring node has when updating a node's feature representation. Unlike traditional GNNs, which aggregate information from all neighbors equally, GAT learns to focus on the most relevant ones, improving the accuracy of its predictions.

As shown in Figure 2a, the proposed architecture consists of 5 GAT layers. The first four layers each have 32 neurons and four self-attention heads. The fifth layer contains as many neurons as there are target classes and operates with a single self-attention head. This specific five-layer architecture was empirically identified as the optimal configuration through our comprehensive Neural Architecture Search (NAS), described in Section 6.4. This search determined the best balance between model complexity and performance from a wide range of possibilities. The output of the final layer is passed to the output layer Y . For each node, the network returns the probability that it belongs to one of the TS segments. All hidden layers use the Exponential Linear Unit (ELU) activation function, while the final layer uses a softmax function. The ELU activation function manages the negative input values from the TS and contributes to model convergence and accuracy.

5.2 Selected baseline models

SotA DL TSS approaches, such as seq2seq⁸, focus on sliding window methods, limiting granularity due to their fixed size. To overcome this and allow fair comparison to our proposed dense labeling approach, our baseline is based on the sequence2point (seq2point) DL model²⁹, which is an adaptation of seq2seq. This version avoids window-based segmentation constraints by predicting a single midpoint element of a window.

The architecture of the baseline DL model is depicted in Figure 2b. The input TS window is fed into five consecutive one-dimensional convolutional layers. First layer consists of 30 kernels of size 10, second of 30 kernels of size 8, third of 40 kernels of size 6, followed by two layers consisting of 50 kernels of size 5. The output of the last convolutional layer is fed into a fully connected or Dense layer consisting of 1024 node units, which is then connected to the output layer of size Y , where the softmax activation function is applied and the classification is made. The size of the Y depends on the number of different classes present in the used dataset. All convolutional layers have a stride of 1, while both convolutional and Dense layers employ the Rectified Linear Units (ReLU) activation function.

To benchmark our approach against SoTA unsupervised techniques, we employ the CLaP (Time Series State Detection) method³⁰. Unlike simple CPD, which only localizes structural breaks, CLaP addresses the broader task of Time Series State Detection (TSSD): identifying and localizing recurring latent states within unannotated time series. In our implementation, we realize this state detection pipeline in two stages. First, we utilize ClaSP¹⁵, a parameter-free change point detector that exploits self-supervised learning to identify optimal segment boundaries based on classification accuracy. Once the time series is partitioned into distinct segments, we perform the state identification step by extracting a vector of statistical features for each segment (mean, standard deviation, minimum, maximum, and linear slope). These segment descriptors are then grouped using K-Means clustering to assign a discrete semantic state label to each segment. To ensure a rigorous evaluation of the method's descriptive capability, the number of clusters k is set to match the ground truth number of classes for each dataset.

6 Methodology and experimental details:

To outline the specifics of our work, first we explain the process of dataset preparation and then show the details of model training and evaluation processes.

6.1 Dataset

We validated our method using the TSSB dataset¹⁵. This dataset contains 75 annotated univariate TS with between 1 and 9 segments. Following common evaluation methodologies in TSS, we excluded TS containing only one segment, as they inherently lack change points and thus do not provide meaningful information about our method's segmentation performance. Furthermore, TS containing duplicated segments were also discarded, since the dataset only contains the change point locations without the labels of each segment. As a result, our final dataset included 59 different TSSB datasets covering various domains, ensuring that our method is domain agnostic.

For our proposed method, each of the datasets was transformed into different graph representations as outlined in Section 4. For the seq2point baseline model, we applied a sliding window approach with a window length of 51 samples. Due to the limited length of certain TSSB datasets, this provided the best balance between the number of samples that could be used to train the model and the performance of the model. The center points of each window were labeled. The window was moved along the entire length of the TS dataset with a step of 1 so that the labels were assigned to all points. Due to the windowing process, the first and last 25 points of the TS had to be excluded to prevent loss of critical information.

6.2 Model training and evaluation

For training our proposed model for the node classification task, we utilized a standard node masking approach to split the dataset into training and testing sets with an 80:20 ratio. For each dataset within TSSB, we applied random node masking three separate times using different seeds. The model was then trained using only the nodes included in the training mask, and its performance was evaluated on the test nodes. A similar 80:20 split approach was used to train the baseline seq2point model, ensuring that both models follow the same data partitioning strategy. Each model was trained and tested five times with different random seeds, and the final performance results are reported as the average of these runs to account for variability in the random splits.

Given that our datasets are imbalanced, where the number of instances in different classes is not equal, we assigned weights to the classes during the training process. The weights were calculated based on the inverse proportion of each class in the dataset. By assigning higher weights to the minority classes and lower weights to the majority classes, the model is forced to pay more attention to the minority ones. Otherwise, it gets higher penalties if it misclassifies them. The models were trained for 1500 epochs using batch size 1 to process the graph as a whole.

For evaluating performance, we relied on the standard F1 score for each class, calculated as: $F1\ score = \frac{2 \times \text{Precision} \times \text{Recall}}{\text{Precision} + \text{Recall}}$, where: $\text{Precision} = \frac{\text{TP}}{\text{TP} + \text{FP}}$, $\text{Recall} = \frac{\text{TP}}{\text{TP} + \text{FN}}$, and TP, FP and FN stand for true positives, false positives and false negatives.

6.3 Comparative Analysis of Training Sample Ratios

To further highlight the advantages of our proposed model over the baseline, especially in terms of performance and data efficiency, we conducted an additional experiment in which we analyze the effects of different train-test split ratios. The experiment was conducted utilizing random shuffle splits across a range of ratios from 10:90 to 90:10 with a step of 10. At each split, the experiments were repeated three times. The experiment highlights one of the main advantages of our approach: it achieves higher model performance with considerably less training data, as described in Section 7.3.

6.4 Ablation study

To understand the nuanced contributions and significance of individual architectural components, we conducted a rigorous ablation study. Adopting a methodical approach, this study was structured as a comprehensive Neural Architecture Search (NAS) to systematically discern the relative influence of key hyperparameters on the trade-off between model performance and computational complexity. The NAS was implemented as a multi-objective optimization using the Optuna framework's NSGAIISSampler, simultaneously aiming to minimize the total number of model parameters and maximize the Mean F1-Score. This process enables the identification of a Pareto front of optimal solutions, revealing the functional dependencies between model size and classification accuracy.

The search space was designed to thoroughly investigate the model's structural limitations. We evaluated network depth by varying the number of GATConv layers from 2 to 6, and network width by sampling hidden dimensions from 32, 64, 96, 128, 160, 192. To determine the optimal node aggregation strategy, we incorporated a comparison of attentive and non-attentive mechanisms directly into the search space. We examined the complexity of the attention mechanism by varying the number of GAT heads from 2, 4, 6, 8, while also evaluating a structural baseline in which the GAT layers were replaced with standard Graph Convolutional Network (GCN) layers. By including both architectures in the same optimization process, we could directly benchmark the value of dynamic neighbor weighting against static convolution under identical training constraints.

Additionally, the NAS optimized key training hyperparameters, including the learning rate, sampled from a log-uniform distribution between 5×10^{-4} and 3×10^{-3} , and the weight decay regularization, chosen from a categorical selection of $\{0.0, 1 \times 10^{-4}, 1 \times 10^{-3}\}$. All configurations were trained and evaluated on our comprehensive global panel, which consists of 59 time series.

7 Results

In this section, we evaluate graph-based frameworks for TSS, using the experimental setup detailed in Section 6. We first assess the overall viability of the approach by benchmarking the GAT model, combined with the transformations listed in Table 2, against two baselines: the unsupervised ClaSP + K-Means and the supervised seq2point model. These aggregated results across the full 59-dataset TSSB benchmark are presented in Figure 3.

Second, we examine how model performance correlates with the intrinsic complexity of the time series. To test this, we analyze the results by grouping datasets according to their number of segments, from 2 to 7, as shown in Figures 4-8. Finally, we assess generalization under data-constrained conditions by analyzing the impact of varying train-test split ratios on the leading WDPVG transformation relative to both baselines.



Figure 3. Combined overall performance across all the datasets

7.1 Overall model performances

Figure 3 shows the overall performance of all implemented TSS methods across 59 univariate TSSB datasets. Each boxplot summarizes the distribution of performance scores for a given TS to graph transformation combined with the GAT model, except for the first two boxplots, which represent the baseline models. From left to right, the next 22 boxplots correspond to different VG transformations, followed by 5 boxplots for Transition networks, and the last one for a Proximity network. The central line in each boxplot represents the median, while the top and bottom edges indicate the 75th and 25th percentiles, forming the interquartile range (IQR). The whiskers extend up to 1.5 times the IQR, and all points outside the whiskers are considered outliers. In this context, higher medians and narrower boxes generally indicate stronger and more consistent performance. Of all the models evaluated, the WDPVG, the simple NVG, and the weighted NVG variants achieved the best results.

The first boxplot from the left in Figure 3 represents the unsupervised ClaSP + K-Means baseline. While it achieves a competitive median score, the distribution reveals significant instability. The box is considerably wider than the top-performing graph methods, and the bottom whisker extends deeply, indicating large failures on specific datasets. This performance dispersion highlights the limitation of statistical baselines. While they excel at detecting clear trend changes or amplitude shifts, they struggle to generalize across datasets characterized by complex texture or subtle morphological changes.

The second boxplot represents the seq2point baseline. It shows a relatively good performance with a median F1 score of approximately 0.93. The IQR extends roughly between 0.85 and 0.98. Compared to the stronger NVG-based approaches, this baseline model is less stable and more sensitive to fluctuations in specific datasets, as evidenced by notable outliers around 0.8 and 0.55.

In contrast, the WDPVG method, shown in the third boxplot, achieves the strongest overall performance compared to both baselines and other graph transformations. This aligns with the expectations outlined in Section 4, regarding the advantages of the WDPVG transformation, specifically its ability to capture additional structural information through its dual perspective. The median F1 score is positioned very high, close to 0.98. Combined with the narrowest IQR and short whiskers, this suggests both superior performance and exceptional stability. This indicates that the WDPVG transformation consistently captures underlying patterns and change points across diverse signal domains, marking it as the most robust transformation for the TSS task.

Comparing the undirected and unweighted NVG, shown in the fourth boxplot, with the weighted NVG variants shown in boxplots 5-8, we observe a very similar overall performance. The median values across all variants are consistently above 0.9, with a similarly narrow IQR. This suggests that topological or structural features have more influence on the segmentation process than edge weights. Edges define the overall structure of the graph by connecting data points, while edge weights primarily influence how these relationships are interpreted rather than altering the topology itself.

Boxplots 9-16 in Figure 3 represent the NVG variants with assigned edge directions. The left-to-right orientation outperforms the top-to-bottom direction, aligning naturally with the sequential order of TS data. Furthermore, we see that all directed variants exhibit higher variability and a greater number of outliers than their undirected counterparts. This is because directionality constrains the way the nodes in the graph are connected. In undirected VGs, every node is equally visible in both directions, whereas directed VGs filter out certain connections. As a result, the model misses out on useful structural information provided by the backward visibility.

Compared to the more successful NVG-based methods, the HVG variants listed in boxplots 17 to 23 exhibit a greater dispersion of performance scores and a higher number of outliers. This increased variability is not surprising, as the horizontal line of sight can oversimplify the relationships between data points, potentially overlooking important structural transitions. Consequently, the HVGs' median performance values often fall below those of the NVGs, approximately around the value 0.85, and their wider IQRs and long extending whiskers suggest less consistency across different datasets.

Finally, the MTF and proximity transformations, shown in boxplots 24 to 29, resulted in a complex network representation that makes the detection of significant structures practically impossible in our TSS task. As illustrated in Figure 3, these transformations produce the lowest median values and have some of the widest IQRs compared to all other transformations. The probabilistic nature of these transformations not only captures the noise in the data but also smooths out sudden changes or local fluctuations that are crucial for accurate segmentation³¹.

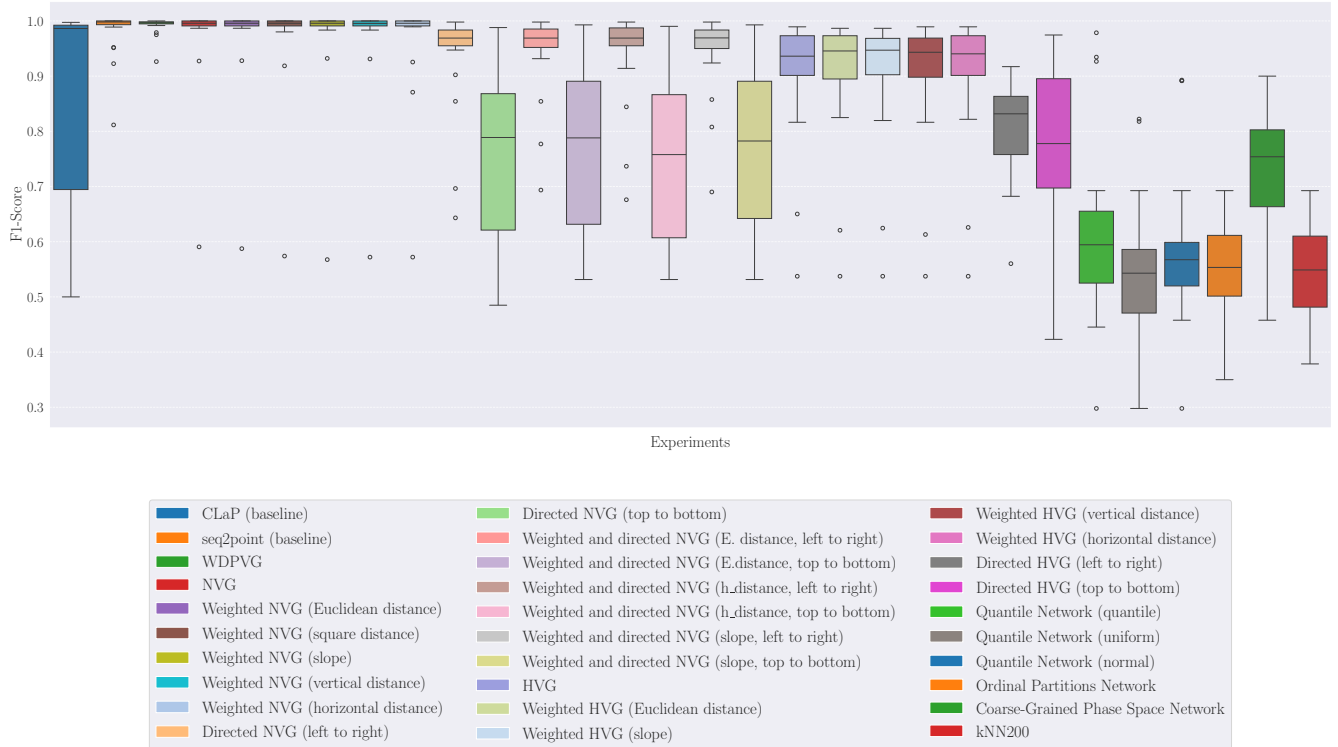


Figure 4. Boxplot summarizing the F1 score variability across various network architectures for 2-segment datasets.

7.2 Performance comparison based on number of segments

In this subsection, we evaluate the performance of the leading graph-based transformation WDPVG against both the supervised seq2point baseline and the unsupervised ClaSP + K-Means baseline across datasets with varying numbers of segments. We specifically focus on the WDPVG, NVG, and baseline model, since NVG is foundational to WDPVG. Other models discussed previously have been analyzed in detail in Section 7.1.

Figure 4 illustrates the results for the 21 datasets containing two segments. In this simpler binary segmentation task, the performance landscape is mixed. The ClaSP + K-Means baseline, shown in the first boxplot, demonstrates high potential with a median near 1.0 but suffers from extreme instability, indicated by a very wide IQR and a whisker extending down to 0.5. This suggests it either solves the task perfectly or fails significantly depending on the dataset. The seq2point baseline shows more stability but a slightly lower median. Both WDPVG and NVG, represented as the third and fourth boxplots, exhibit highly competitive and stable performance, with medians approaching 1.0 and very narrow IQRs, proving their robustness even in



Figure 5. Boxplot summarizing the F1 score variability across various network architectures for 3-segment datasets.

simple scenarios.

As complexity increases in datasets with three segments, the graph-based methods begin to distinguish themselves, as shown in Figure 5. WDPVG achieves a dominant median F1 score of approximately 0.98 with a tight IQR (0.95–0.99), indicating superior stability. The ClaSP baseline shows a low median, and remains the most volatile method, with a boxplot that spans a wide range of performance scores. The seq2point baseline drops, with a median around 0.92 and increased variability. NVG maintains strong performance with a median near 0.98, positioning it as a solid intermediate between the baselines and WDPVG.

In Figure 6, the results for four-segment datasets further highlight the robustness of WDPVG. The WDPVG model maintains exceptional performance with a median of roughly 0.99 and negligible variability (IQR 0.98–1.0). The ClaSP baseline shows improved stability compared to the two- and three-segment scenarios. iT achieves a high median near 1.0 and a tighter interquartile range, though it still exhibits a long lower whisker extending down to approximately 0.68, indicating occasional underperformance. The seq2point baseline performs reliably with a median around 0.95, but displays a wider spread than the graph-based methods. NVG remains highly competitive, mirroring WDPVG's high median performance, albeit with a slightly increased number of outliers.

For datasets with five segments (Figure 7), performance is highly competitive across all methods. WDPVG and NVG remain top performers, both achieving medians effectively at 1.0 with negligible variance. Notably, the ClaSP + K-Means baseline also demonstrates exceptional stability in this specific category, matching the graph methods with a median near 1.0 and a narrow IQR, though it exhibits outliers down to 0.8. The seq2point baseline shows marked improvement, reaching a median close to 0.99 with a tight distribution, yet similarly suffers from distinct performance drops.

Finally, in the most complex scenarios with six or seven segments (Figure 8), WDPVG demonstrates its scalability, achieving a median of nearly 0.99 with consistently low variability (IQR 0.98–1.0). NVG also performs strongly, though with slightly lower consistency than WDPVG. Conversely, the seq2point baseline falls behind with a median of 0.88 and significant variability. The ClaSP baseline exhibits its characteristic instability, with a high median but a distribution that suggests frequent failures. These results confirm that WDPVG is particularly effective for complex, multi-segment tasks, capturing structural dependencies that purely statistical or sequential baselines often miss.

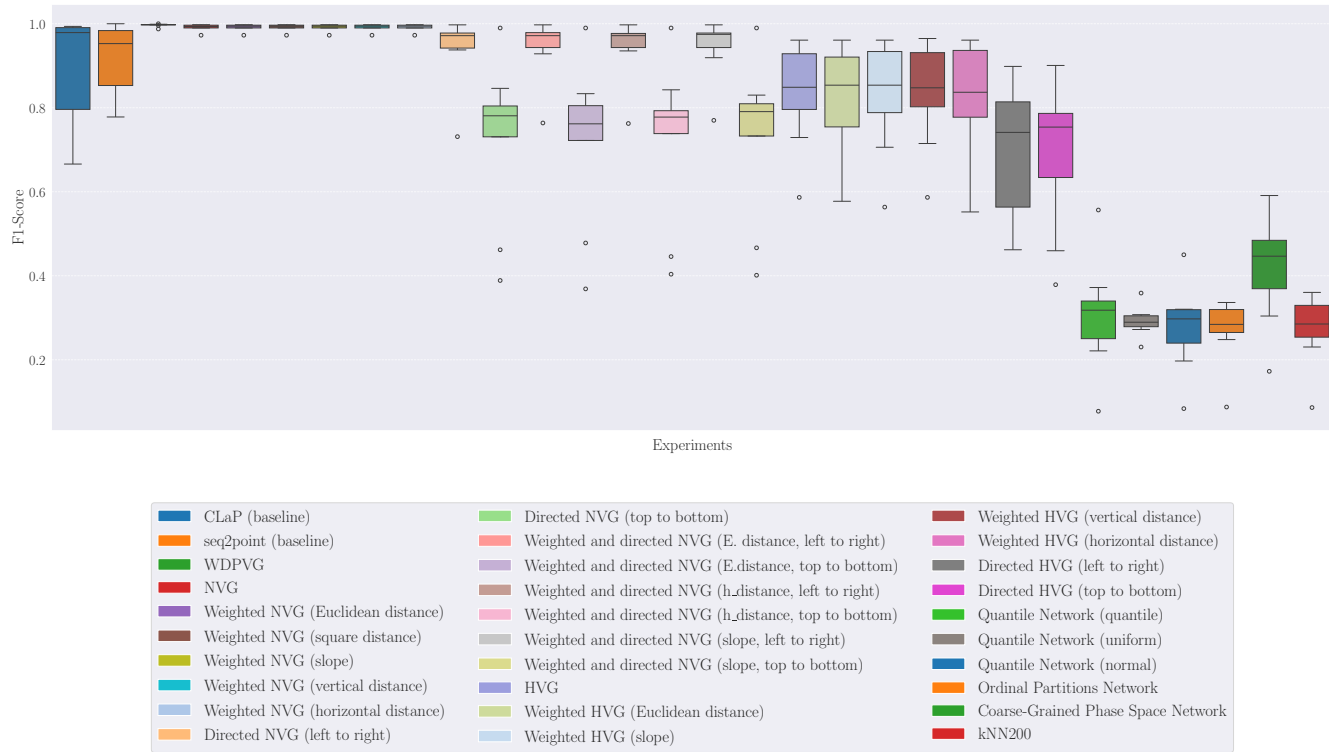


Figure 6. Boxplot summarizing the F1 score variability across various network architectures for 4 segment datasets.

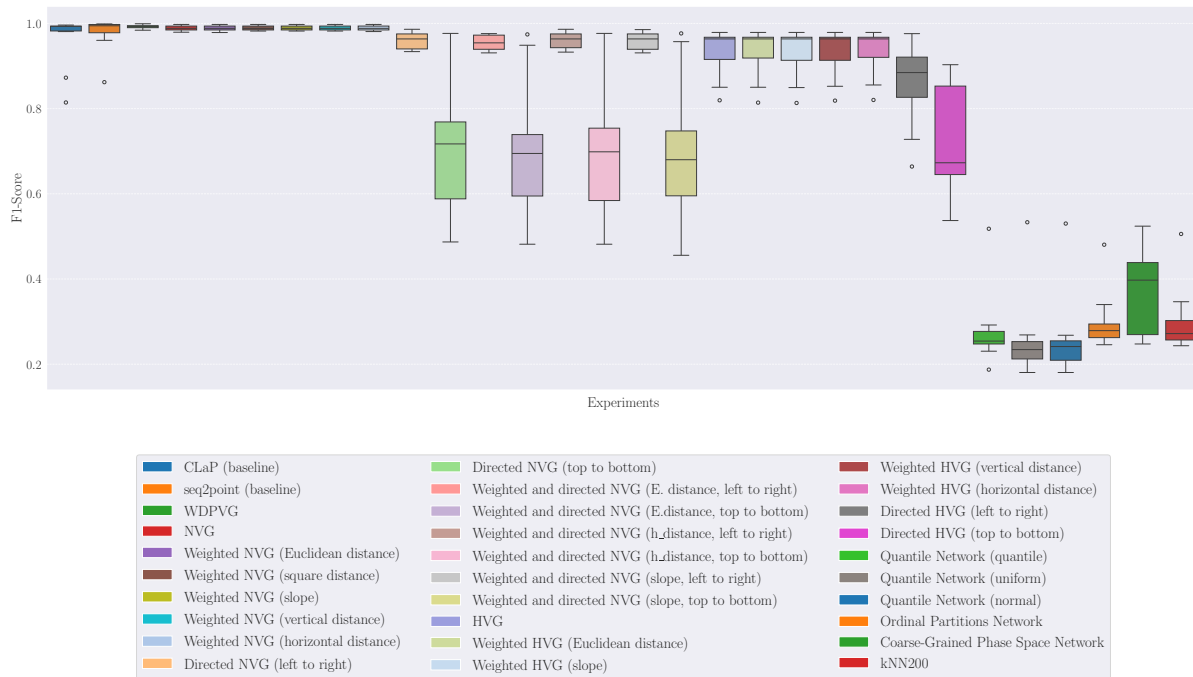


Figure 7. Boxplot summarizing the F1 score variability across various network architectures for 5 segment datasets.

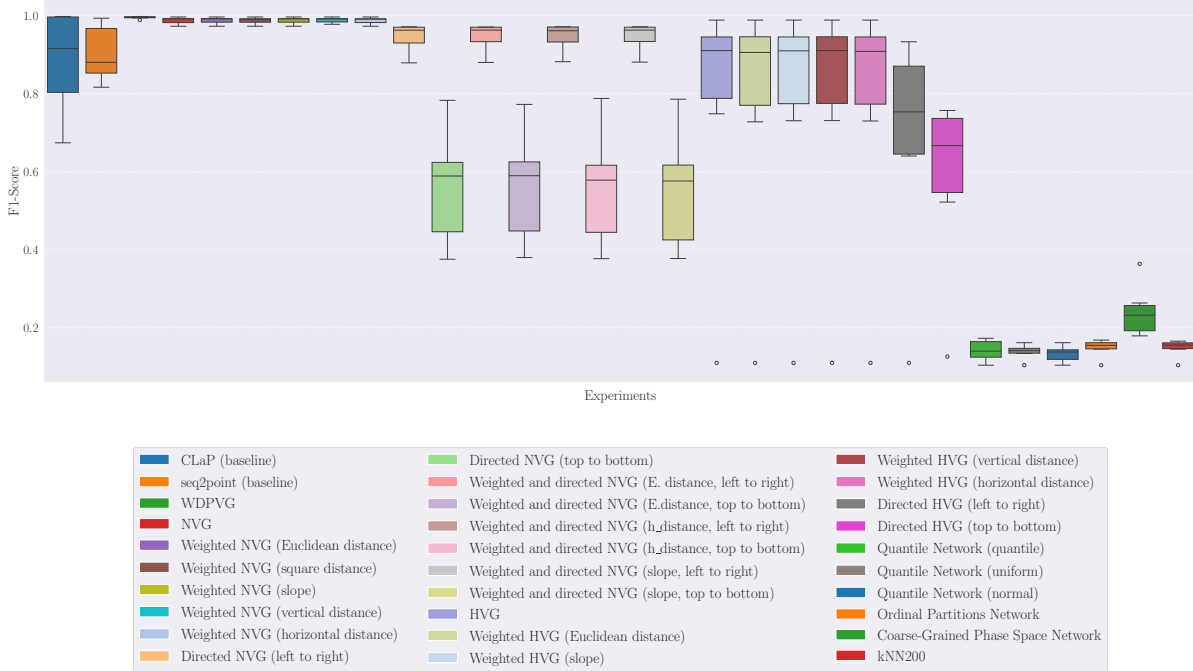


Figure 8. Boxplot summarizing the F1 score variability across various network architectures for 6 and 7 segment datasets.

7.3 Analysis of Training Sample Ratios on Model Performance

To evaluate the effect of the number of training samples on classification performance, we compared the proposed WDPVG-based model and the baseline model using the methodology described in Section 6. Figure 9 illustrates how the ratio of training to testing data impacts the model’s performance. The graph displays the average weighted F1 scores across all 59 datasets. As expected, the F1 scores for both the proposed and baseline models gradually improve as the proportion of training data increases. Also, this figure highlights the advantages of our approach. Even when using a fraction of only 10% of the available data for training, it achieves an impressive average F1 score of 0.95, significantly outperforming the baseline score of 0.73. This trend continues also for other ratios, which proves that our approach requires considerably less training data to achieve higher model performance compared to the baseline.

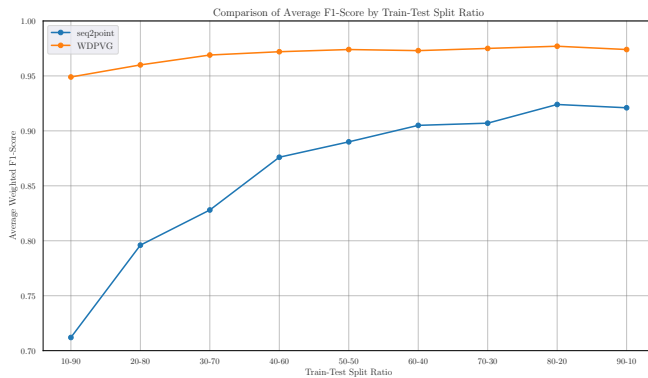


Figure 9. Impact of different train-test split ratios on the TSS model performance across TSSB datasets

Additionally, we compared the number of trainable parameters between the proposed and baseline model. As shown in Table 3, our proposed model has ≈ 22 times fewer weights compared to the seq2point baseline (0.053M vs. 1.174M). This demonstrates that our graph-based approach achieves significantly higher parameter efficiency, delivering superior average F1 scores across all datasets with a fraction of the model complexity.

Model	Number of trainable weights
WDPVG	$\approx 0.053M$
seq2point	$\approx 1.174M$

Table 3. Model trainable weights

comparison

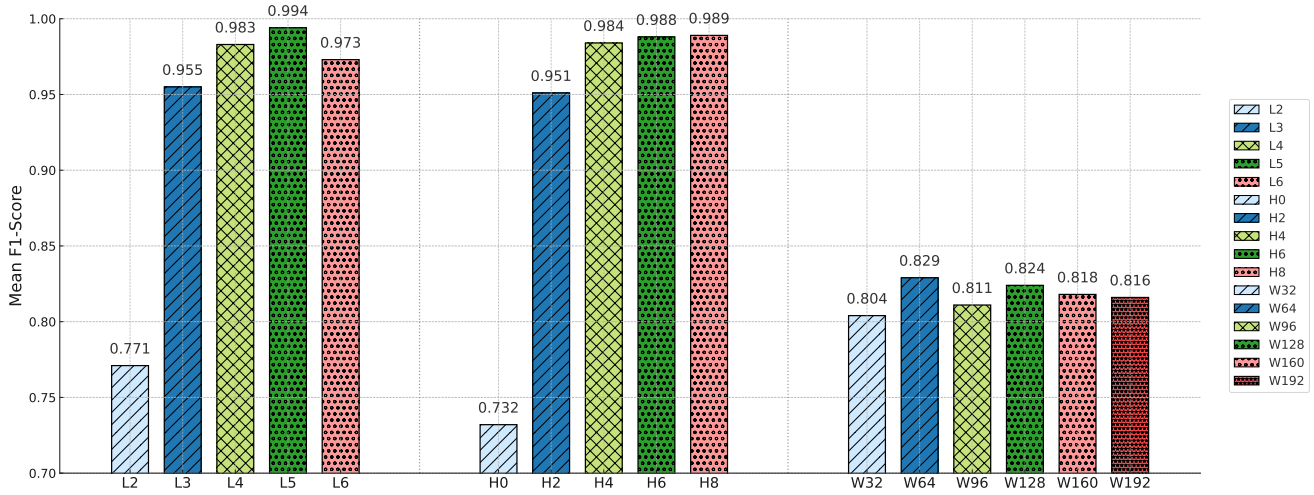


Figure 10. Marginal impact of architectural components—Depth (L), Attention Heads (H), and Hidden Dimension (W)—on the mean F1-score across all search trials.

7.4 Ablation study results

Following the methodology detailed in Section 6.4, our Neural Architecture Search (NAS) identified a Pareto front of optimal architectures that effectively balance the trade-off between model complexity and performance. These non-dominated solutions are summarized in Table 4. Each entry represents a configuration where no other discovered solution achieves a higher F1-score without a simultaneous increase in parameter count.

To understand the structural properties that drive high performance along this Pareto front, we analyzed the marginal contribution of each architectural component across all search trials. These dependencies are visualized in Figure 10.

Crucially, the results reveal that **architectural depth** is the primary determinant of performance. As illustrated in the left panel of Figure 10, increasing network depth (L) from 2 to 5 layers yields the most significant performance gain. Models limited to a depth of 2 layers (L2) averaged an F1-score of only 0.771, whereas increasing the depth to 5 layers (L5) pushed the performance to a near-perfect 0.994. This structural necessity is reflected in the Pareto front (Table 4), where every top-performing configuration (Trials 89, 93, 66) utilizes a depth of at least 5 layers. This confirms that a deeper receptive field is essential for capturing the long-range temporal dependencies required for accurate segmentation.

Secondly, the comparison between Graph Attention (GAT) and Graph Convolutional (GCN) architectures quantifies the critical role of the attention mechanism. As shown in the center panel of Figure 10 and detailed in Table 5, the attention mechanism (H) significantly outperforms the non-attentive GCN baseline (H0), which achieved a mean F1-score of only 0.732. Conversely, utilizing just 2 attention heads (H2) jumps the performance to 0.951. This substantial gap of over 20 percentage points validates our hypothesis: the dynamic neighbor weighting provided by GATs is not merely an optimization, but a functional requirement for solving the dense labeling problem in this domain. Unlike GCNs, which aggregate information from all neighbors equally, GATs can effectively filter out noisy or irrelevant connections inherent in VGs.

Finally, the right panel of Figure 10 provides crucial insight into parameter efficiency regarding the hidden dimension width (W). While increasing the width to 64 units (W64) yields a peak mean F1-score of 0.829, outperforming the W32 configuration (0.804), the performance gain is marginal relative to the increase in model complexity. Beyond W64, the metric plateaus or even slightly degrades. Consequently, we selected the W32 configuration for the final architecture. The slight trade-off in raw performance is justified by the substantial reduction in parameter count, validating our preference for "thin and deep" architectures that maximize efficiency without compromising the model's ability to capture essential features.

Synthesizing these structural insights, we selected **Trial 66** (Table 4) as our final optimized architecture. While Trial

Trial	Layers	Hidden Dim.	Heads	Learning Rate	Weight Decay	Params (M)	Mean F1
68	2	32	2	2.3×10^{-3}	0.0	0.001	0.732
78	2	32	4	3.0×10^{-3}	0.0003	0.001	0.795
70	2	32	6	1.3×10^{-3}	0.0003	0.002	0.821
50	2	64	6	1.2×10^{-3}	0.0	0.003	0.829
27	3	32	2	2.3×10^{-3}	0.0	0.005	0.898
36	4	32	2	1.0×10^{-3}	0.0001	0.010	0.951
89	5	32	2	5.7×10^{-4}	0.0001	0.014	0.960
93	6	32	2	8.2×10^{-4}	0.0	0.019	0.984
66	5	32	4	5.1×10^{-4}	0.0	0.053	0.995

Table 4. Pareto front solutions from the NAS, detailing the trade-off between model parameters and mean F1-score.

93 represents the efficient "knee" of the curve (0.019M params, 0.984 F1), Trial 66 leverages the optimal combination of depth (5 layers) and attention (4 heads) to achieve a peak F1-score of 0.995. We deemed the increase in the number of trainable parameters acceptable given the precision gains. Notably, this optimized model remains approximately 22× more parameter-efficient than the baseline seq2point model (≈ 1.17 M parameters), validating the superiority of the graph-based approach.

Model	Mean Precision	Mean Recall	Mean F1-Score
GCN	0.741	0.740	0.732
GAT	0.995	0.995	0.995

Table 5. Performance comparison of the optimized GAT model against the GCN ablation baseline, averaged across all datasets.

8 Conclusions

In this paper, we introduced a novel TSS approach that transforms time series data into graphs via the WDPVG and utilizes Graph Attention Networks (GAT) for segment classification. We also conducted an extensive study on various transformations of time series—into graphs—including simple and weighted visibility graphs as well as transition and proximity networks—and analyzed their strengths and limitations for TSS. Based on our findings, we conclude the following:

- Our proposed WDPVG consistently exhibits superior performance, achieving an average F1 score of 0.97 in 59 benchmark datasets. By capturing both peaks and troughs and addressing uneven sampling, WDPVG effectively preserves important structural information in time series.
- We validated the proposed method with the TSSB repository, which includes datasets from different domains such as gesture recognition, ECG recordings, and sensor-based measurements. The consistently high performance in these different contexts underlines the broad applicability of our approach.
- Our work demonstrates how transforming time series into graphs can improve a model’s ability to capture complex and wide-ranging relationships—particularly beneficial for multi-segment scenarios. By integrating graph representations with a Graph Attention Network, we achieve an F1 improvement of about 0.05 over a strong seq2point baseline.
- An important practical advantage lies in the data efficiency of our method. It requires significantly fewer labeled samples to converge while maintaining competitive accuracy. This makes the approach particularly attractive when working with large datasets that have limited labeled data.
- Experiments also show that the WDPVG exhibits high stability, even for dynamic datasets with potential noise and abrupt shifts. This resilience stems from the dual visibility perspective, which enriches the graph’s connectivity and improves the GNN’s ability to learn unique segment boundaries.

Overall, our study demonstrates that combining graph-based time-series transformations with GNN architectures can significantly improve TSS. By effectively capturing both the temporal and topological features of time series, our WDPVG and

GAT approach not only consistently achieves higher segmentation accuracy, but also generalizes well across different domains. We anticipate that these findings will drive further research to develop advanced graph-based methods for various time series analysis tasks.

Acknowledgements

This work was supported by the Slovenian Research Agency (P2-0016) and the European Commission NANCY project (No. 101096456).

References

1. Carvalho, T. P. *et al.* A systematic literature review of machine learning methods applied to predictive maintenance. *Comput. & Ind. Eng.* **137**, 106024 (2019).
2. Qaddoura, R., M. Al-Zoubi, A., Faris, H. & Almomani, I. A multi-layer classification approach for intrusion detection in iot networks based on deep learning. *Sensors* **21**, 2987 (2021).
3. Khan, S. & Yairi, T. A review on the application of deep learning in system health management. *Mech. Syst. Signal Process.* **107**, 241–265 (2018).
4. Gers, F. A., Schmidhuber, J. & Cummins, F. Learning to forget: Continual prediction with lstm. *Neural computation* **12**, 2451–2471 (2000).
5. Aghabozorgi, S., Shirkhorshidi, A. S. & Wah, T. Y. Time-series clustering—a decade review. *Inf. systems* **53**, 16–38 (2015).
6. Lebedev, I. & Rzayev, B. Segmentation of data when analyzing the state of telecommunication systems. *Indonesian J. Electr. Eng. Comput. Sci.* **29**, 1473–1479 (2023).
7. Perslev, M., Jensen, M., Darkner, S., Jenum, P. J. & Igel, C. U-time: A fully convolutional network for time series segmentation applied to sleep staging. *Adv. neural information processing systems* **32** (2019).
8. Phan, H., Andreotti, F., Cooray, N., Chén, O. Y. & De Vos, M. Seqsleepnet: End-to-end hierarchical recurrent neural network for sequence-to-sequence automatic sleep staging. *IEEE Transactions on Neural Syst. Rehabil. Eng.* **27**, 400–410, DOI: [10.1109/TNSRE.2019.2896659](https://doi.org/10.1109/TNSRE.2019.2896659) (2019).
9. Zheng, M., Domanskyi, S., Piermarocchi, C. & Mias, G. I. Visibility graph based temporal community detection with applications in biological time series. *Sci. reports* **11**, 5623 (2021).
10. Lacasa, L., Luque, B., Ballesteros, F., Luque, J. & Nuno, J. C. From time series to complex networks: The visibility graph. *Proc. Natl. Acad. Sci.* **105**, 4972–4975 (2008).
11. Luque, B., Lacasa, L., Ballesteros, F. & Luque, J. Horizontal visibility graphs: Exact results for random time series. *Phys. Rev. E Statistical, Nonlinear, Soft Matter Phys.* .
12. Supriya, S., Siuly, S., Wang, H., Cao, J. & Zhang, Y. Weighted visibility graph with complex network features in the detection of epilepsy. *IEEE access* **4**, 6554–6566 (2016).
13. Shen, W. *et al.* A survey on label-efficient deep image segmentation: Bridging the gap between weak supervision and dense prediction. *IEEE transactions on pattern analysis machine intelligence* **45**, 9284–9305 (2023).
14. Arif, S. N. A. M., Mohsin, M. F. M., Bakar, A. A., Hamdan, A. R. & Abdullah, S. M. S. Change point analysis: a statistical approach to detect potential abrupt change. *J. Teknologi* **79** (2017).
15. Ermshaus, A., Schäfer, P. & Leser, U. Clasp: parameter-free time series segmentation. *Data Min. Knowl. Discov.* **37**, 1262–1300 (2023).
16. De Ryck, T., De Vos, M. & Bertrand, A. Change point detection in time series data using autoencoders with a time-invariant representation. *IEEE Transactions on Signal Process.* **69**, 3513–3524 (2021).
17. Gaugel, S. & Reichert, M. Prectime: A deep learning architecture for precise time series segmentation in industrial manufacturing operations. *Eng. Appl. Artif. Intell.* **122**, 106078 (2023).
18. Veličković, P. *et al.* Graph Attention Networks. *Int. Conf. on Learn. Represent.* (2018).
19. Silva, V. F., Silva, M. E., Ribeiro, P. & Silva, F. Time series analysis via network science: Concepts and algorithms. *Wiley Interdiscip. Rev. Data Min. Knowl. Discov.* **11**, e1404 (2021).
20. Ghosh, S. K. *Visibility algorithms in the plane* (Cambridge university press, 2007).

21. Lacasa, L., Nunez, A., Roldán, É., Parrondo, J. M. & Luque, B. Time series irreversibility: a visibility graph approach. *The Eur. Phys. J. B* **85**, 1–11 (2012).
22. de Oliveira Campanharo, A. S. L. & Ramos, F. M. Quantile graphs for the characterization of chaotic dynamics in time series. In *2015 Third World Conference on Complex Systems (WCCS)*, 1–4 (Ieee, 2015).
23. Donner, R. V. *et al.* Recurrence-based time series analysis by means of complex network methods. *Int. J. Bifurc. Chaos* **21**, 1019–1046 (2011).
24. Zhang, J. & Small, M. Complex network from pseudoperiodic time series: Topology versus dynamics. *Phys. review letters* **96**, 238701 (2006).
25. Zhang, J., Luo, X. & Small, M. Detecting chaos in pseudoperiodic time series without embedding. *Phys. Rev. EStatistical, Nonlinear, Soft Matter Phys.* **73**, 016216 (2006).
26. Yang, Y. & Yang, H. Complex network-based time series analysis. *Phys. A: Stat. Mech. its Appl.* **387**, 1381–1386 (2008).
27. Marwan, N. A historical review of recurrence plots. *The Eur. Phys. J. Special Top.* **164**, 3–12 (2008).
28. Veličković, P. *et al.* Graph attention networks. *arXiv preprint arXiv:1710.10903* (2017).
29. Zhang, C., Zhong, M., Wang, Z., Goddard, N. & Sutton, C. Sequence-to-point learning with neural networks for non-intrusive load monitoring. In *Proceedings of the AAAI conference on artificial intelligence*, vol. 32 (2018).
30. Ermshaus, A., Schäfer, P. & Leser, U. Clap–state detection from time series. *arXiv preprint arXiv:2504.01783* (2025).
31. Wang, Z. & Oates, T. Encoding time series as images for visual inspection and classification using tiled convolutional neural networks. In *Workshops at the twenty-ninth AAAI conference on artificial intelligence* (2015).

APPENDIX

In this section, we summarize the detailed performance results presented in Tables 6 to 10, where each table groups datasets by the same number of classes or distinct segments. The first column lists the dataset names, while the remaining columns present the selected metrics for the proposed WDPVG method, the Euclidean distance-weighted NVG transformation combined with our proposed model, and the baseline seq2point model. The final two rows in each table report the Mean and Standard Deviation (STD) of these metrics for each dataset subset.

As shown in Table 6, the proposed method outperforms the other models for 2-segment tasks. It achieves the highest Mean F1 score of 0.991, compared to 0.972 for NVG and 0.976 for seq2point. The proposed method achieves a higher or equal F1 score than seq2point in 12 out of 21 datasets, and a higher or equal score than NVG in 15 out of 21 datasets. The proposed method demonstrates particular robustness on difficult datasets (such as ChlorineConcentration and DistalPhalanxOutlineAgeGroup), contributing to its superior overall Mean score.

In Tables 7 and 8, the proposed method continues to outperform both NVG and the seq2point baseline. For 3-class segmentation, shown in Table 7, it achieves a Mean F1 score of 0.945 (compared to 0.936 for NVG and 0.833 for seq2point) and secures a higher or equal F1 score than NVG in 11 out of 13 datasets and than seq2point in 10 out of 13 datasets. This trend remains strong for 4-class segmentation, shown in Table 8, where the proposed method achieves the highest F1 score in 8 out of 9 datasets compared to seq2point, yielding a near-perfect Mean F1 score of 0.996.

In Table 9, the proposed method maintains its strong performance, achieving the highest Mean F1 score of 0.993 (compared to 0.990 for NVG and 0.973 for seq2point). The baseline method achieves a higher score only on 'UWaveGestureLibraryAll' and 'SyntheticControl'.

Finally, Table 10, which includes datasets with 6 or 7 segments, confirms that our proposed method is particularly suitable for tasks with a higher number of segments. It outperforms the seq2point baseline in all 6 datasets. The proposed method achieves the highest Mean F1 score of 0.994, demonstrating its effectiveness in capturing complex structural dependencies.

Overall, the results show that the proposed method is the most reliable and high-performing model across all levels of segmentation complexity, from 2 to 7 classes.

Dataset (num. segm.)	Proposed method			ClaSP + KMeans			seq2point		
	Prec.	Rec.	F1	Prec.	Rec.	F1	Prec.	Rec.	F1
ArrowHead (2)	0.99890	0.99888	0.99899	0.99280	0.99269	0.992695	0.97522	0.97374	0.97373
Beef (2)	0.99646	0.99645	0.99645	0.98687	0.98652	0.98652	0.99756	0.99754	0.99755
BeetleFly (2)	0.99806	0.99805	0.99805	0.98780	0.98750	0.98749	0.99803	0.99801	0.99802
BirdChicken (2)	1.00000	1.00000	1.00000	0.99689	0.99687	0.99688	0.99675	0.99661	0.99668
ChlorineConcentration (2)	0.90768	0.90284	0.90438	0.48558	0.69683	0.57233	0.91049	0.89684	0.88789
Coffee (2)	0.99670	0.99666	0.99667	0.99701	0.99700	0.99699	0.99826	0.99825	0.99824
Computers (2)	0.99617	0.99615	0.99616	0.25000	0.50000	0.33333	0.95503	0.95416	0.95415
DistalPhalanxOutlineAgeGroup (2)	0.99656	0.99650	0.99651	0.96587	0.96433	0.96307	0.66265	0.81401	0.73056
ECG200 (2)	0.99586	0.99583	0.99583	0.98572	0.98541	0.98532	0.99925	0.99923	0.99921
ECGFiveDays (2)	0.99582	0.99573	0.99576	0.99745	0.99744	0.99744	0.99778	0.99775	0.99773
GunPoint (2)	0.99476	0.99467	0.99469	0.97803	0.97707	0.97703	0.99374	0.99366	0.99360
ItalyPowerDemand (2)	0.99586	0.99591	0.99589	0.99265	0.99254	0.99253	1.00000	1.00000	1.00000
Lightning2 (2)	0.99587	0.99583	0.99581	0.44444	0.66666	0.53334	0.99571	0.99563	0.99560
MedicalImages (2)	0.99933	0.99931	0.99932	0.99136	0.99111	0.99114	0.98693	0.98695	0.98594
MoteStrain (2)	0.99901	0.99902	0.99900	0.99237	0.99226	0.99226	0.99696	0.99693	0.99695
SonyAIBORobotSurface1 (2)	0.99421	0.99405	0.99407	0.99083	0.99071	0.99067	0.99635	0.99629	0.99627
SonyAIBORobotSurface2 (2)	0.99906	0.99905	0.99905	0.98663	0.98632	0.98628	0.99709	0.99706	0.99706
ToeSegmentation1 (2)	0.99941	0.99939	0.99940	0.76467	0.59711	0.52136	0.99939	0.99937	0.99938
ToeSegmentation2 (2)	0.99785	0.99783	0.99784	0.75238	0.55832	0.45322	0.99891	0.99889	0.99890
TwoLeadECG (2)	0.98640	0.98565	0.98596	0.27279	0.52229	0.35839	1.00000	1.00000	1.00000
Yoga (2)	0.96976	0.96975	0.96973	0.8169	0.69450	0.67305	0.98986	0.98974	0.98962
Mean	0.99113	0.99084	0.99093	0.83948	0.86064	0.82292	0.97362	0.98003	0.97558
STD	0.02020	0.02121	0.02089	0.25303	0.17865	0.23354	0.07424	0.04475	0.06159

Table 6. Classification results of the proposed model compared to the baselines for 2-class segmentation.

Dataset (num. segm.)	Proposed method			ClaSP + KMeans			seq2point		
	Prec.	Rec.	F1	Prec.	Rec.	F1	Prec.	Rec.	F1
CBF (3)	0.97590	0.97396	0.97417	0.98976	0.98958	0.98955	0.99639	0.99633	0.99633
CinCECGTorso (3)	0.99699	0.99698	0.99697	0.52290	0.50857	0.43927	0.83061	0.82350	0.82386
DiatomSizeReduction (3)	1.00000	1.00000	1.0000	0.54821	0.53673	0.47361	0.81082	0.80455	0.80109
DistalPhalanxTW (3)	0.98452	0.99449	0.98447	0.73358	0.84147	0.78007	0.58136	0.73188	0.63292
Haptics (3)	0.98620	0.98608	0.98609	0.15631	0.39536	0.22405	0.92194	0.92068	0.92028
InlineSkate (3)	0.99862	0.99863	0.99861	0.45923	0.54076	0.44911	0.83934	0.83525	0.83491
LargeKitchenAppliances (3)	0.99725	0.99723	0.99724	0.49735	0.65587	0.54770	0.91888	0.91855	0.91854
Meat (3)	0.98969	0.98978	0.98959	0.62183	0.48303	0.46246	0.91099	0.90483	0.90367
OliveOil (3)	0.49697	0.40328	0.37505	0.66643	0.66086	0.63333	0.59613	0.51947	0.38795
OSULeaf (3)	0.99606	0.99598	0.99600	0.99480	0.99471	0.99472	0.99919	0.99917	0.99918
ProximalPhalanxOutlineAgeGroup (3)	0.99545	0.99541	0.99542	0.68465	0.74775	0.704415	0.91310	0.90337	0.90459
Trace (3)	0.99804	0.99802	0.99803	0.98042	0.97994	0.97986	0.91620	0.91104	0.90971
WordSynonyms (3)	0.99111	0.99095	0.99099	0.71489	0.84551	0.77473	0.73821	0.85936	0.79496
Mean	0.95437	0.94775	0.94482	0.65926	0.70616	0.65022	0.84409	0.85600	0.83292
STD	0.13761	0.16374	0.17135	0.23933	0.20172	0.24336	0.13428	0.12542	0.16479

Table 7. Classification results of proposed model compared to the baseline for 3-class segmentation.

Dataset (num. segm.)	Proposed method			ClaSP + KMeans			seq2point		
	Prec.	Rec.	F1	Prec.	Rec.	F1	Prec.	Rec.	F1
Adiac (4)	1.000	1.000	1.000	0.73414	0.67471	0.67175	0.90071	0.91911	0.90474
Car (4)	0.99547	0.99538	0.99539	0.69140	0.79611	0.72904	0.94417	0.94089	0.94077
FaceFour (4)	0.99862	0.99863	0.99861	0.98922	0.98917	0.98916	0.85255	0.88463	0.86533
FiftyWords (4)	0.99659	0.989647	0.99654	0.99333	0.99326	0.99326	0.99677	0.99676	0.99675
InsectWingbeatSound (4)	0.99616	0.99608	0.99610	0.97984	0.97890	0.97890	0.99360	0.99325	0.99325
Mallat (4)	0.99291	0.99286	0.9929	0.99376	0.99369	0.99367	0.76916	0.82100	0.78026
ProximalPhalanxTW (4)	0.98409	0.98375	0.98377	0.99133	0.99075	0.99088	0.68450	0.80717	0.73971
SwedishLeaf (4)	0.99810	0.99809	0.99808	0.91286	0.88534	0.87694	0.97865	0.97832	0.97835
Symbols (4)	0.99826	0.99825	0.99824	0.84345	0.66596	0.62701	0.94647	0.94475	0.94167
Mean	0.99558	0.99550	0.99551	0.90326	0.88532	0.87229	0.89629	0.92065	0.90454
STD	0.00478	0.00488	0.00487	0.12200	0.13437	0.14732	0.10846	0.07025	0.09264

Table 8. Classification results of the proposed model compared to the baselines for 4-class segmentation.

Dataset (num. segm.)	Proposed method			ClaSP + KMeans			seq2point		
	Prec.	Rec.	F1	Prec.	Rec.	F1	Prec.	Rec.	F1
CricketX (5)	0.99624	0.99623	0.99622	0.99365	0.99353	0.99353	0.995	0.99616	0.99616
CricketY (5)	0.99246	0.99241	0.99243	0.98683	0.98666	0.98665	0.98274	0.98236	0.98234
CricketZ (5)	0.99516	0.99510	0.99512	0.99337	0.99337	0.99337	0.98550	0.98501	0.98492
Lightning7 (5)	0.99543	0.99542	0.99541	0.78671	0.87261	0.82217	0.86212	0.86106	0.85634
ShapesAll (5)	0.99844	0.99842	0.99843	0.99373	0.99359	0.99359	0.98105	0.98031	0.98037
SyntheticControl (5)	0.99382	0.99379	0.99377	0.99551	0.99546	0.99546	0.99955	0.99955	0.99955
UWaveGestureLibraryAll (5)	0.97951	0.97928	0.97933	0.996613	0.99609	0.99610	0.97348	0.99940	0.99940
UWaveGestureLibraryX (5)	0.99120	0.99113	0.99116	0.99336	0.99325	0.993226	0.98673	0.98676	0.97129
UWaveGestureLibraryY (5)	0.99653	0.99645	0.99647	0.98191	0.98084	0.98096	0.97348	0.97111	0.97129
UWaveGestureLibraryZ (5)	0.9930	0.99525	0.99527	0.72013	0.814407	0.75203	0.97661	0.97593	0.97585
Mean	0.99341	0.99335	0.99336	0.94418	0.96198	0.95071	0.97433	0.97377	0.97330
STD	0.00530	0.00536	0.00535	0.10185	0.06409	0.08792	0.04046	0.04076	0.04220

Table 9. Classification results of the proposed model compared to the baselines for 5-class segmentation.

Dataset (num. segm.)	Proposed method			ClaSP + KMeans			seq2point		
	Prec.	Rec.	F1	Prec.	Rec.	F1	Prec.	Rec.	F1
NonInvasiveFetalECGThorax1 (6)	0.99639	0.99637	0.99638	0.99735	0.99734	0.99734	0.87522	0.86297	0.86213
NonInvasiveFetalECGThorax2 (7)	0.99107	0.99103	0.99102	0.99725	0.99723	0.99724	0.88387	0.90718	0.89291
FaceAll (7)	0.99675	0.99677	0.99676	0.71970	0.67371	0.62776	0.99111	0.99049	0.99051
FacesUCR (7)	0.99462	0.99460	0.99461	0.78491	0.79114	0.76723	0.83795	0.90262	0.86606
Fish (7)	0.98723	0.98714	0.98717	0.99242	0.99229	0.99230	0.88477	0.88668	0.88238
Plane (7)	0.99607	0.99603	0.99602	0.79975	0.83783	0.80558	0.85076	0.91197	0.87684
Mean	0.99369	0.99366	0.99366	0.88190	0.88159	0.86458	0.88728	0.91032	0.89514
STD	0.00379	0.00382	0.00381	0.13093	0.13627	0.15497	0.05424	0.04313	0.04803

Table 10. Classification results of the proposed model compared to the baselines for 6 and 7-class segmentation.